Colour Logging as a Tool in High Resolution Palaeoceanography.

M. Rogerson*‡, P.P.E Weaver*, E. J. Rohling*, L. J. Lourens†, J.W. Murray* and A. Hayes§.

* Southampton Oceanography Centre, European Way, Southampton, SO14 3ZH, UK

† Faculty of Geoscience, University of Utrecht, Budapestlaan, 4, 3584 CD, Utrecht, Netherlands

§ Department of Geology, Royal Holloway College, Egham, Surrey, TW20 0EX, UK

‡ Corresponding author:- now at Faculty of Geoscience, University of Utrecht, Netherlands;

email:- rogerson@geo.uu.nl

Abstract

Colour and diffuse reflectance records can be used to develop astronomically tuned age models for long sediment cores. Here, we present high resolution (1mm) colour records from a sediment core from the western Gulf of Cadiz of southwest Spain (D13892), spanning the last deglaciation, in parallel with stable isotope ($\delta^{18}O$) and Sea Surface Temperature proxy data. The age model is based on $\delta^{18}O$ stratigraphy complemented by 5 AMS radiocarbon datings. We find good comparison between the colour record of D13892 and the GISP2 oxygen isotope series ($R^2 = 0.81$), which strongly suggests that the sediment colour reflects the state of the climate. As sediment colour variability has previously been found to be diagnostic of changes in mineralogical / chemical composition, we relate the causes of the colour variability in D13892 to changes in the local particle flux, and support these observations with data from core logging XRF analyses. The colour and XRF-logger records for D13892 suggest that the last glaciation and Younger Dryas were characterised by enhanced

supply of terrigenous detritus into the western Gulf of Cadiz. Cyclicities with wavelengths of 607 and 1375 years are recognised in the colour records for the Holocene. This cyclicity also relates to variability in detrital supply, with an important eolian component implied by enrichment in haematite during cycle maxima.

Colour has been considered to be diagnostic of the composition of soils for several decades (Goddard et al. 1948), and this concept is now increasingly being applied to marine sediments (eg. Mix et al., 1992). Geochemical investigation of sediment core material has shown that aspects of colour (eg. lightness) are reliable indicators of important sedimentological components such as carbonate, free and bound iron, a variety of Fe minerals (e.g. haematite, pyrite, goethite) and clay. The dominant redox state of iron, be it within minerals or as ions (particularly within the lattice of clay minerals), can also be reliably estimated from colour (Mix et al. 1992; Nagao and Nakashima 1992; Mix et al. 1995; Balsam and Deaton 1996; Giosan et al. 2002).

Greyscale (lightness) has successfully been used for initial chronostratigraphic model development within long sediment cores, especially those collected by the Ocean Drilling Program (Ortiz et al. 1999; Grutzner et al. 2002). It is rapidly and easily measured and dominantly controlled by the carbonate content, though TOC is also important, which is thought to be regulated by orbitally modulated insolation (Hays and Peruzza 1972; Volat et al. 1980; Ortiz et al. 1999). Recently, a combined investigation of geochemistry and sediment colour has shown systematic variability in mineralogical and carbonate content, both predicted by colour, on Milankovitch and sub-Milankovitch (~1.5kyr) wavelengths (Grutzner et al. 2002). This indicates a

potential for the use of colour as a means of developing initial chronostratigraphic models for high-resolution records from the late Quaternary. Here, we investigate this potential using sediment colour, geochemical, stable isotope and planktonic foraminiferal abundance records for a sediment core (D13892) from the western Gulf of Cadiz (southwest Spain), with an independent age model based on 5 radiocarbon datings and $\delta^{18}O$ isotope stratigraphy.

Study Area

The Gulf of Cadiz (GoC) lies to the southwest of the Iberian Peninsula, immediately west of the Strait of Gibraltar (fig. 1). The exchange of Mediterranean and Atlantic water through the Strait of Gibraltar drives the formation of two currents that are present within the GoC (Bryden et al. 1988). The shallow, eastward component of this flow compensates for water lost from the Mediterranean by evaporation and by the deep, westward outflow (the Mediterranean Outflow, MO). Within the GoC, the Atlantic Inflow current flows along the shelf from northwest to southeast, elongating the sedimentary deposits formed at the mouths of the Iberian rivers along the northern and eastern margins of the GoC (Bryden et al. 1988; Lopez-Galindo et al. 1999). The subsurface Mediterranean Outflow (MO) is a plume of relatively warm and saline dense water that, after its exit from the Strait of Gibraltar, passes along the GoC slope between 500 and 1500m water depth. It interacts with the sea floor from Cape Spartel in the south-east to Cape St. Vincent in the north-west (Kenyon and Belderson 1973; Ambar and Howe 1979; Iorga and Lozier 1999), where it profoundly influences the nature of sedimentation. Material is transported along the slope from the southeast to the northwest (Kenyon and Belderson 1973). In the southeast, where the flow is strongest, the path of the current is characterised by abrasion surfaces and sand ribbons, which fine north-westwards as the flow decelerates, to become sandy and

then muddy sediment drifts (Kenyon and Belderson 1973). Suspended material is transported in suspension out into the western GoC, to areas where the MO no longer interacts with the sea floor (Ambar et al. 2002).

On the upper slope of the GoC, where the flow is at least partially in contact with the sea floor, the MO plume is characterised by significantly higher suspended particulate matter (SPM) content than the Atlantic water it is passing through (Ambar et al. 2002). This SPM comprises both mineral and biogenic grains, the biogenic component being dominantly calcareous. Further offshore, the SPM content of water in the MO plume is significantly decreased, and more comparable to Atlantic water than to the Mediterranean water found close to the shelf (Ambar et al. 2002). There, SPM is generally <10μm in diameter and the biogenic component is dominantly siliceous (Ambar et al. 2002). This indicates that the majority of the SPM transported by the Mediterranean Outflow is deposited close to the region of supply where the plume interacts with the sea floor, and relatively little is transported into the western GoC today. Variability in the supply of sediment to the MO plume and in its capability to transport SPM (primarily its internal turbulence) would be reflected by variability in detrital material supply at the core location.

The GoC region is arid and characterised by strong and stable winds, especially the easterly Levanter and northerly trade winds (Dorman et al. 1995). Today, Levanter winds trap air pollution and dust close to the ground and cause visibility to decrease by as much as 30%. During the summer, the trade winds are strong, stable and active >50% of the time at the city of Cadiz (Fiuza et al. 1982). It is likely that the western GoC experiences a significant supply of aeolian detritus via these wind regimes. If the

local wind field has been variable in the past, it is anticipated that this would have some impact on sedimentation at the core location.

Material and Methods

Core D13892 is a 2m long kasten core recovered from the western Gulf of Cadiz, from a water depth of 1500m, during RRS *Discovery* cruise 249. This location lies beyond the region where the Mediterranean Outflow interacts with the sea floor, and there is no indication of either current or turbidite activity in this core. Five radiocarbon datings have been performed on >6mg of planktonic foraminiferal tests (*Globigerina bulloides, Globigerinoides ruber, Globigerinoides sacculifer*) picked from the >150μm fraction. The radiocarbon analyses were undertaken via the NERC Radiocarbon Laboratory (NERC-RCL), at the University of Arizona NSF-AMS facility.

For the planktonic foraminiferal abundance study, samples were disaggregated in demineralised water, washed and sieved to remove all material finer than 150μm. Where necessary, samples were then split into suitable aliquots of at least 300 individuals for identification according to the taxonomy of Hemleben et al. (1989). The data are presented as percentages of total planktonic foraminiferal number. Planktonic foraminifera assemblages were analysed by Artificial Neural Network (ANN) to produce estimates of summer and winter sea surface temperature (Malmgren et al. 2000). The training set used was based on core top samples from both the North Atlantic and the Mediterranean, as the GoC lies between these two basins.

The specimens selected for stable isotope analyses are washed and sonicated in methanol to remove surface contamination. For each sample stable isotope analyses were carried out on 7-15 individuals of dextral coiling *Neogloboquadrina pachyderma* between sizes of 150 and 212μm. Stable isotope analyses were carried out using a Europa Geo 2020 mass spectrometer with individual acid dosing method at the SOES facility in Southampton. The carbon and oxygen isotope ratios are expressed as δ values, in per mils (‰), relative to the Vienna Peedee Belemnite standard, (Coplen 1988; Coplen 1994).

Colour analysis and XRF scanning

Core-section surfaces were first smoothed with a glass slide and then imaged using a GEOSCAN colour line scan camera. This device uses a 3 x 1024 pixel CCD (charge-coupled device) array that measures absolute red, green, and blue (RGB) colour intensities to produce a finely pixelated image of the sediment surface. A value of 255 in each wavelength band is calibrated to a standard white. Average RGB values are measured for each pixel ($14\mu m^2$), which are then combined into bitmap files for each core section. The bitmap files are compiled in the Geoscan software (www.geotek.co.uk/site/scripts/module.php?webSubSectionID=28) to form a continuous image for the whole core, into which sub-surface depth data is incorporated.

A panel of the image covering a whole core, core section or part of a section is then selected manually in the Geoscan software. Downcore resolution within this panel is set manually at any level up to a best resolution of 100μm. Data for D13892 have been produced at 1mm resolution. Average values for red (450-490mm), green (500-550mm) and blue (590-660mm) are automatically calculated for each 1mm interval

across the width of the selected interval. Numerical RGB data is then linked to the depth of the top of the measured interval from the core-top in mm and complied as downcore reflectance records for each of the three wavelength bands. RGB reflectance values may be expressed either as mean reflectance in each of the wavelength bands ("Absolute Reflectance") or as the relative contribution of each wavelength band to the total reflectance at that depth ("Relative Reflectance"). Data is then exported from the Geoscan software as an ASCII file. The uppermost part of the core (subsequent to 10ka BP) was selected for spectral analysis using the ARfit package (Paillard et al. 1996), to give insight into cyclicities underlying the colour variability.

Additional analyses were performed using a Minolta Spectrophotometer. Ten samples were taken from the core, oven dried and ground to a fine powder. This powder was poured into a well cut into a sheet of cardboard and the surface smoothed prior to analysis, to remove errors due to differences in water content and surface unevenness. Spectral data was pre-treated by differentiation to increase the variance (as proposed by Giosan et al., 2002) and is presented as curves showing the first differential of reflectance across the visible light spectrum.

Here we use the lightness (L), chroma (C) and hue (H) system to parameterise colour (Giosan et al. 2002). Lightness has been shown in numerous studies to be sensitive to the carbonate composition (Mix et al. 1992; Nagao and Nakashima 1992; Mix et al. 1995; Giosan et al. 2002). Hue and chromaticness have been shown to be sensitive to the content and redox state of iron (Giosan et al. 2002). However, the response of colour to chemical and mineralogical changes is non-linear, and quantitative

estimation of sediment composition is difficult. Here, colour data are supported by chemical data produced by X-ray fluorescence (XRF) analysis.

The core sections were analysed with the Cox Analytical Systems Itrax XRF core logger at Southampton Oceanography Centre. This system uses capillary optics to focus an X-Ray beam produced from a molybdenum filament onto the surface of a split core. A stepper motor moves the core in 400μm increments, and at each increment the core is irradiated. The atomic fluorescences produced are collected by an analyser close to the surface of the core and the intensity of fluorescence peaks at registered wavelengths are recorded for each step. Thus, a 400μm resolution record is produced of relative elemental abundances. Here, only data for Fe and Ca are reported.

Spectral analysis

Power spectra were obtained by using the CLEAN transformation of Roberts et al. (1987) in the ARfit package. The CLEAN technique is an iterative deconvolution method that involves trial fitting curves of a range of different frequencies to the data series. The height of spectral peaks therefore represent the probability that a significant periodicity of that wavelength exists in the data. For the determination of errors associated with the frequency spectra of the CLEAN algorithm, we applied the Monte Carlo based method developed by Heslop and Dekkers (2002). The 97.5% and 99.5% significance levels for the Monte Carlo spectra were determined by 1) 10% red noise addition (i.e., Control parameter = 0.1), 2) “Clean Gain factor” (Heslop and Dekkers, 2002) of 0.1, 3) 500 CLEAN Iterations, 4) The sample spacing for the interpolated data series (dt) was set at 5 years, and 5) 500 simulation iterations.

Chronostratigraphic Framework

The radiocarbon dates were calibrated to calendar ages using the OXCAL program (www.rlaha.ox.ac.uk/orau/oxcal.html), assuming a 400 year reservoir age. Figure 2 shows the position of the calibrated radiocarbon dates, the probability distribution of their calibrations to calendar age, and the 95% confidence interval of possible age-depth correlations. An initial chronostratigraphic model is derived (shown in black), which represents the smoothest line of best fit between peaks of high probability.

It is very likely that major events, such as the warming at the termination of the last glaciation and the start and end of the Younger Dryas, are synchronous between this location, and the wider GoC and Iberian margin (Bard et al. 1987; Lebreiro et al. 1997; Cayre et al. 1999; Bard et al. 2000; Shackleton et al. 2000; Thomson et al. 2000; Cacho et al. 2001; Moreno et al. 2002; Schönfeld et al. 2003) and so with the North Atlantic and Greenland in general. The chronostratigraphic model for D13892 is therefore fine-tuned by correlating these events in the D13892 $\delta^{18}O$ record to the GISP2 $\delta^{18}O$ series, and these relationships are supported by the SST record. Figure 3 shows the SST and oxygen isotope data on this final chronostratigraphic model relative to the GISP2 isotope series, with the correlation points marked. The adjustment made to the chronostratigraphic framework during the fine-tuning process is generally small (individual corrections were <500years (see Table 1)). The final chronostratigraphic model used is shown as the broken line in Figure 2.

Results

Figure 4d-f shows RGB and $\delta^{18}O_{N.\ pachyderma\ (d)}$ plots for D13892. As the red, green and blue plots track one another closely, the colour variation is mainly related to lightness

(L). Figure 5 shows the L, C and H records for D13892. Close correspondence of L (Fig. 5b) and absolute reflectance (Fig. 5a) in the D13892 is apparent. L in D13892 correlates to the individual absolute reflectance records with R^2 in excess of 0.99 (N=1814), which confirms that grey-scale reflectance is the underlying control on these data. Spectrophotometry (Fig. 6) indicates that most of the reduction in L between the minimum lightness (glacial) and maximum lightness (Holocene) parts of this core is attributable to a decline in reflectance in the wavelength band associated with carbonate (Giosan et al. 2002). The close relationship found between L and carbonate content in many other sediment cores (Nagao and Nakashima 1992; Mix et al. 1995; Balsam and Deaton 1996; Hughen et al. 1996; Ortiz et al. 1999; Giosan et al. 2002) can therefore be inferred here. The bulk colour changes in the core therefore represent the ratio between carbonate and detrital material supplied to this 1500m deep location. The relative intensity of each of the wavelengths varies slightly along core (Fig. 4a-c), indicating that the colour variation also has a small hue/chroma component. Figure 5d and e show chroma and hue respectively. Close correspondence is found between Chromaticness (5d) and the relative reflectiveness (Fig. 5c) of the red wavelengths (R^2 = 0.74, N=1813).

Discussion

Colour in D13892 as a tool for chronostratigraphy

There is good agreement between changes in $\delta^{18}O_{\textit{N. pachyderma}\ (d)}$ and changes in lightness, with increasing $\delta^{18}O_{\textit{N. pachyderma}\ (d)}$ values generally correlating with relative darkening. This suggests that the history of sediment supply to this location is dominated by general North Atlantic climate changes. There is an even more striking agreement between the reflectivity and the $\delta^{18}O$ GISP2 record which, in places,

appear to correlate on millennial to centennial timescales. The L and GISP2 $\delta^{18}O$ curves are highly significantly correlated, with $R^2 = 0.81$ (N = 413). Colour logging therefore has great potential for the development of initial sediment-core chronostratigraphies. However, there are discrepancies as well. For example, a discrepancy exists between the structures of the colour and GISP2 $\delta^{18}O$ records concerning the expression of the warmest part of the Bölling – Allerød (~14.6ka BP), which seems under-represented in the colour record of D13892.

Origin of colour variability

Figure 7 shows L for D13892, the GISP2 $\delta^{18}O$ series, and chemical data produced by XRF logging of D13892 (Fe/Ca). Fe/Ca can be viewed as the detrital : carbonate ratio, and this curve agrees well with the reflectivity (L) record ($r^2 = 0.65$, N = 1814), giving strong support to our interpretation of the latter as a proxy for carbonate content. High peaks in Fe/Ca occur at the glacial terminations 1a and 1b. In the case of T1a, the start of the Fe/Ca peak coincides with the deglaciation in $\delta^{18}O$ of GISP2, whereas the deglaciation in the colour record of D13892 appears to be delayed. The sharp peak in Fe/Ca values in D13892 likely reflects elevated detrital supply during the deglaciation. A period of high detrital supply would be anticipated to cause depressed reflectivity values during its duration, as is recognised here at T1a. It is therefore probable that the apparent delay of T1a in the colour record of D13892 reflects the impact of ice melt, drainage basin rearrangement and/or changes in the behaviour of the local oceanic currents rather than the state of the climate. Where similar detrital pulses occur in other locations at the time of glacial terminations, the effect on the colour record will cause a potential error for age models developed from astronomical tuning.

The Younger Dryas and glacial parts of the D13892 record exhibit lower lightness, higher Fe/Ca (Fig. 7) and significantly higher accumulation rates than the Holocene (Fig. 2). The number of planktonic foraminiferal tests per gram (dry weight) is low during periods with high rates of accumulation. In the Holocene, the number of tests per gram is of the order of 1000-1600, whereas during the latter part of the Younger Dryas, when deposition was most rapid (Fig. 2), the number of tests per gram is found to be as low ~200. This suite of observations is more consistent with a variable rate of supply of detrital grains to the core location than with variable rate of carbonate production, which would be reflected in reduced accumulation rate during periods of low carbonate content. Cold periods thus exhibit higher detrital supply than warm periods in the D13892 record. Some variation in the rate of carbonate production cannot be ruled out, but the rate of carbonate supply on the Portuguese margin is thought to have been relatively constant over the past 140kyr (Thomson et al. 1999).

During the Holocene part of D13892, the >150μm sediment fraction consists almost exclusively of planktonic foraminiferal tests. Before the Holocene, and particularly during the Younger Dryas, abundant terrigenous grains are found in this fraction as well. These are mainly quartz and lithic clasts, some of them with dark coatings, with abundant mica and some black, oxidised wood fragments. Similar grain assemblages are found in samples from the lowermost part of the MO contourite drift (Gil Eanes drift, Fig. 1) (Habgood et al. 2003; Rogerson 2003). D13892 lies further downstream in the MO pathway than this region, and the petrological similarity between the deposits reflect an important role played by the MO in supplying mineral grains to the western GoC. The large scale colour variablity in D13892 therefore reflects variable

supply of terrigenous grains to this location through time, with the MO probably playing a significant role as a transportation pathway.

Colour variability in the Holocene

The Holocene parts of D13892 exhibit a series of cyclic lightness minima (Fig. 4d-f). Spectral analysis shows spectral peaks at 1375 and 607 years in the Holocene part of this record (younger than 10ka, BP), which are significant at the 97.5% confidence level (Fig. 8). These minima are found across all three absolute reflectance records (Fig. 4d-f), and thus in L, and coincide with maxima in the red and minima in the blue relative reflectance records (Fig. 4a-c). The high chromaticness (Fig. 5d) of these layers will reflect changes in the composition of the sediment itself, likely the enrichment and redox state of the iron present. Several Holocene lightness minima coincide with local maxima in Fe/Ca (Fig. 7), confirming that these represent carbonate depleted/iron enriched layers. These lightness minima therefore reflect short duration (~100-500 years) periods of either increased supply of iron rich mineral detritus, or decreased carbonate productivity. Spectrophotometry indicates that these minima have increased reflectance in the wavelengths associated with haematite relative both to the background Holocene and the last glaciation (Fig 6), which would generally be associated with increased eolian input (Balsam et al. 1995). This suggests that airborne dust may be an important factor governing the Holocene cyclic variability, implicating variability in either atmospheric turbulence or aridity in the region surrounding the GoC during this period.

Conclusions

Colour logging is a useful tool that may be used for producing high-resolution chronostratigraphic frameworks by correlation with well-constrained climatic records. It has potential to be particularly useful as a method of developing initial

chronostratigraphic information for a sediment core in order to develop a sampling strategy for more conventional analyses, as continuous colour logging is a cheap, rapid, non-destructive method of producing very high-resolution data for sediment cores.

The western Gulf of Cadiz experienced an enhanced supply of detrital grains during the Younger Dryas and the latter part of the last glaciation. Greatly enhanced detrital supply is found in the western GoC during the glacial Terminations (1a and 1b). The detritus is petrologically similar to sand found on the Gil Eanes Drift, indicating that it was probably supplied by the Mediterranean Outflow.

Enhanced detrital supply was also found during cyclic periods within the Holocene, with spectral peaks at 607 and 1375 years. Increased haematite content in diluted layers implies increased aeolian dust input as one factor in controlling this cyclicity.

Acknowledgements

We would like to thank Guy Rothwell and Ian Croudace for allowing access to the BOSCORF Itrax scanner, and John Thomson for his help in interpreting the data. Steve Cooke, Matt Cooper and Mike Bolshaw are thanked for performing the stable isotope analyses. NERC-RCL is thanked for providing funding for the radiocarbon dating (project 949.1201), and for performing the analyses. Reviewers A. Nederbragt and L. Giosan are thanked for their comments, which improved the manuscript considerably.

References

Ambar, I., and M.R. Howe, Observations of the Mediterranean Outflow II - The deep circulation in the vaicinity of the Gulf of Cadiz, *Deep-Sea Research*, **26A**, 555-568, 1979.

Ambar, I., N. Serra, M.J. Brogueira, G. Cabecadas, F. Abrantes, P. Freitas, C. Goncalves, and N. Gonzalez, Physical, chemical and sedimentological aspects of the Mediterranean outflow off Iberia, *Deep-Sea Research II*, **49**, 4163-4177, 2002.

Balsam, W.L., and B.C. Deaton, Determining the composition of late Quaternary marine sediments from NUV, VIS and NIR diffuse reflectance spectra., *Marine Geology*, **134**, 31-55, 1996.

Balsam, W.L., B.L. Ottobleisner, and B.C. Deaton, Modern and last glacial maximum eolian sedimentation patterns in the Atlantic-ocean interpreted from sediment iron-oxide content, *Paleoceanography*, **10** (3), 493-507, 1995.

Bard, E., A.J. Arnold, P. Maurice, J. Duprat, J. Moyes, and J.C. Duplessy, Retreat velocity of the North Atlantic polar front during the last deglaciation determined by ^{14}C accelerator mass spectrometry, *Nature*, **328** (6133), 791-794, 1987.

Bard, E., F. Rostek, J.L. Turon, and S. Gendreau, Hydrological impact of Heinrich Events in the Subtropical Northeast Atlantic, *Science*, **289**, 1321-1324, 2000.

Bryden, H.L., E.C. Brady, and R.D. Pillsbury, Flow through the strait of Gibraltar, in *Seminario sobre la Oceanografia fisica del Estracho de Gibraltar*, edited by J.L. Almazan, H.L. Bryden, T. Kinder, and G. Parilla, SECEG, Madrid, 1988.

Cacho, I., J.O. Grimalt, M. Canals, L. Sbaffi, N.J. Shackleton, J. Schönfeld, and R. Zahn, Variability of the western Mediterranean Sea surface temperature during

the last 25,000 years and its connection with the northern hemisphere climatic changes, *Paleoceanography*, **16** (1), 40-52, 2001.

Cayre, O., Y. Lancelot, E. Vincent, and M.A. Hall, Palaeoceanographic reconstructions from planktonic foraminifera off the Iberian Margin: temperature, salinity and Heinrich events, *Paleoceanography*, **14** (3), 384-396, 1999.

Coplen, T.B., Normalization of oxygen and hydrogen isotope data., *Chemical Geology (Isotope Geoscience Section)*, **72**, 293-297, 1988.

Coplen, T.B., Reporting of stable hydrogen, carbon, and oxygen isotopic abundances., *Pure and Applied Chemistry*, **66**, 273-276, 1994.

Dorman, C.E., R.C. Beardsley, and R. Limeburner, Winds in the Strait of Gibraltar, *Quarterly Journal of the Meteorological Society*, **121**, 1903-1921, 1995.

Fiuza, A.F.G., M.E. Macedo, and M.R. Guerreiro, Climatological space and time variation of the Portuguese coastal upwelling, *Oceanologica Acta*, **5** (1), 31-40, 1982.

Giosan, L., R.D. Flood, and R.C. Aller, Palaeoceanographic significance of seidment color on western North Atlantic drifts: I, Origin of color, *Marine Geology*, **189**, 25-41, 2002.

Goddard, M.B., R.M. Overbeck, O.N. Rove, J.T. Singewald, and P.D. Trask, *Rock-Color Chart*, 6 pp., National Research Council, Washington D.C., 1948.

Grutzner, J., L. Giosan, S.O. Franz, R. Tiedemann, E. Cortijo, W.P. Chaisson, R.D. Flood, S. Hagen, L.D. Keigwin, S. Poli, D. Rio, and T. Williams, Astonomical age models for Pleistocene drift sediments from the western North Atlantic (ODP Sites 1055-1063). *Marine Geology*, **189**, 5-23, 2002.

Habgood, E., N.H. Kenyon, D.G. Masson, A. Akhmetzhanov, P.P.E. Weaver, J. Gardner, and T. Mulder, Deep-water sediment wave fields, bottom current sand channels and gravity flow channel-lobe systems: Gulf of Cadiz, NE Atlantic, *Sedimentology*, **50**, 1-27, 2003.

Hays, J.D., and A. Peruzza, The significance of calcium carbonate oscillations in the eastern equatorial Atlantic deep-sea sediments for the end of the Holocene warm interval, *Quaternary Research*, **2**, 355-362, 1972.

Hemleben, C., M. Spindler, and O.R. Anderson, *Modern Planktonic Foraminifera*, 363 pp., Springer-Verlag, 1989.

Hernandez-Molina, J., E. Llave, L. Somoza, M.C. Fernandez-Puga, A. Maestro, R. Leon, T. Medialdea, A. Barnolas, M. Garcia, V.D.d. Rio, L.M. Fernandez-Salas, J.T. Vazquez, F. Lobo, J.M. Alverinho-Dias, J. Rodero, and J. Gardner, looking for clues to palaeoceanogrpahic imprints: A diagnosis of the Gulf of Cadiz contourite depositional systems, *Geology*, **31** (1), 19-22, 2003.

Heslop, D., and M. Dekkers, Spectral analysis of unevenly spaced climatic time series using CLEAN: signal recovery and derivation of significance levels using a Monte Carlo simulation, *Physics of the Earth and Planetary Interiors*, **130** (1-2), 103-116, 2002.

Hughen, K.A., J.T. Overpeck, L.C. Peterson, and S. Trumbore, Rapid climate changes in the tropical Atlantic region during the last deglaciation, *Nature*, **380**, 51-54, 1996.

Iorga, M.C., and M.S. Lozier, Signatures of the Mediterranean outflow from a North Atlantic climatology 1. Salinity and density fields, *Journal of Geophysical Research*, **104** (C11), 25,985-26,009, 1999.

Kenyon, N.H., and R.H. Belderson, Bed forms of the Mediterranean Undercurrent Observed with Side-Scan sonar, *Sedimentary geology*, **9**, 77-99, 1973.

Lebreiro, S.M., J.C. Moreno, F.F. Abrantes, and U. Pflaumann, Productivity and paleoceanography on the Tore seamount (Iberian margin) during the last 225 kyr: Foraminiferal evidence, *Paleoceanography*, **12** (5), 718-272, 1997.

Lopez-Galindo, A., J. Rodero, and A. Maldonado, Subsurface facies and sediment dispersal patterns: southeastern Gulf of Cadiz, Spanish continental margin, *Marine Geology*, **155**, 83-98, 1999.

Malmgren, B.A., M. Kucera, J. Nyberg, and C. Waelbrock, Comparison of statistical and artificial neural network techniques for estimating past sea surface temperatures from planktonic foraminifera census data, *Paleoceanography*, **16** (5), 520-530, 2000.

Mix, A., S. Harris, and T.R. Janecek, Estimating lithology from nonintrusive reflectance spectra: Leg 138, *Proceedings of the Ocean Drilling Program, Scientific results*, **138**, 413-427, 1995.

Mix, A.C., W. Rugh, N.G. Pisias, S. Veirs, and L.S. Party, Color reflectance spectroscopy: A tool for rapid characterization of Deep-Sea sediments, *Proceedings of the Ocean Drilling Program, Initial Reports 1*, **138**, 67-76, 1992.

Moreno, E., N. Thouveny, D. Delanghe, I.N. McCave, and N. Shackleton, Climatic and oceanographic changes in the Northeast Atlantic reflected by magnetic properties of sediments deposited on the Portuguese margin during the last 340ka., *Earth and Planetary Science Letters*, **202**, 465-480, 2002.

Nagao, S., and S. Nakashima, The factors controlling vertical color variations of North Atlantic Madeira Abyssal Plain sediments, *Marine Geology*, **109**, 83-94, 1992.

Ortiz, J., A. Mix, S. Harris, and S. O'Connell, Diffuse spectral reflectance as a proxy for percent carbonate content in North Atlantic sediments, *Paleoceanography*, **14** (2), 171-186, 1999.

Paillard, D., L. Labeyrie, and P. Yiou, Macintosh program performs time-series analysis, *EOS*, **77**, 379, 1996.

Roberts, D.H., J. Lehar, and J.W. Dreher, Time Series Analysis with Clean - Part One - Derivation of a Spectrum, *Astronomical Journal*, **93** (4), 968, 1987.

Rogerson, M., Palaeoceanography and Sedimentology of the Gulf of Cadiz; 30-0ka BP., PhD thesis, University of Southampton, Southampton, 2003.

Schönfeld, J., R. Zahn, and L. deAbreu, Surface and deep water repsonce to rapid claimate changes at the Western iberian margin., *Global and Planetary Change*, **36** (4), 237-264, 2003.

Shackleton, N., M.A. Hall, and E. Vincent, Phase relationships between millennial-scale events 64,000-24,000 years ago, *Paleoceanography*, **15** (6), 565-569, 2000.

Thomson, J., S. Nixon, C.P. Summerhayes, E.J. Rohling, J. Schönfeld, R. Zahn, P. Grootes, F. Abrantes, L. Gaspar, and S. Vaqueiro, Enhanced productivity on the Iberian margin during glacial/interglacial transitions revealed by barium and diatoms, *Journal of the Geological Society, London*, **157**, 667-677, 2000.

Thomson, J., S. Nixon, C.P. Summerhayes, J. Schönfeld, R. Zahn, and P. Grootes, Impications for sedimentation changes on the Iberian margin over the last two

glacial/interglacial transitions from $(^{230}TH_{excess})_0$ systematics, *Earth and Planetary Science Letters*, **165**, 255-270, 1999.

Volat, J.-L., L. Pastouret, and C. Vergnaud-Grazzini, Dissolution and carbonate fluctuations in Pleistocene deep-sea cores: a review, *Marine Geology*, **34**, 1-28, 1980.

Table 1A

Sample depth (cm)	Conventional radiocarbon age	1σ	Predicted calendar age
8	5647	45	6010
56.7	10429	56	11210
71	10868	59	12040
110	10868	58	12660
173	14353	76	16800

Table 1B

Tie point depth (cm)	Event	Calibrated radiocarbon age	Age in GISP2 chronology
33.1	Warming subsequent to 8.2kyr event	8577	8100
61.7	Termination1b	11349	11700
100	Termination of Bölling-Allerød	12594	13000
136.7	Termination 1a	14416	14600
146	Local $\delta^{18}O$ minimum	14971	15400
152	Local $\delta^{18}O$ maximum	15333	15800
166	Local $\delta^{18}O$ minimum	16171	16500
170	Local $\delta^{18}O$ minimum	16419	16850
176.3	Local $\delta^{18}O$ maximum	16799	17100

Figure Captions

Figure 1. Modified from Sediment facies of the Gulf of Cadiz contourite drift as revealed by sidescan sonar data. Location of D13892 is indicated. Hernandez-Molina et al., (2003).

Figure 2. Chronostratigraphy for D13892. Unbroken line indicates initial chronostratigraphic model, broken line indicates chronostratigraphy after tuning to GISP2 chronology (see Fig. 3)

Figure 3. Artificial Neural Network Sea Surface Temperature and $\delta^{18}O_{N.\ .pachyderma\ (d)}$ records for D13892 relative to GISP2 $\delta^{18}O$ record. Correlation points are shown.

Figure 4. Relationship of climate proxy and colour records in D13892 with GISP2 isotope series. Grey represents GISP2 $\delta^{18}O$, black represents $\delta^{18}O_{N.\ pachyderma\ (d)}$ for D13892. Coloured lines represent red-green-blue intensities, with upper curves indicating relative contribution to colour and lower curves indicating absolute intensity.

BLACK AND WHITE VERSION

Figure 4. Relationship of climate and colour in D13892 records. Grey area represents GISP2 $\delta^{18}O$. a) Relative intensity (red); b) Relative intensity (green); c) Relative intensity (blue); d) Absolute intensity (red); e) Absolute intensity (green); f) Absolute intensity (blue); g) $\delta^{18}O_{N.\ pachyderma\ (d)}$ for D13892.

Figure 5. Raw and transformed colour data for D13892. a) Absolute intensity in green wavelengths; b) Reflectance (L*); c) Relative Intensity (red); d) Chromaticness (C); e) Hue (H^o)

Figure 6. First differential of reflectance of representative samples from D13892, derived from Minolta spectrophotometer measurements. Interpretation of primary controls on reflectance intensities follows Giosan *et al.* 2002. Characteristic peaks in reflectance spectra, identified by statistical analysis of sediment core material analysed by colour and geochemical methods, are found for carbonate (400-500nm), haematite (500-600nm) and the reduced free iron (600-700nm).

Figure 7. Colour, geochemical and tests/gram data for D13892 relative to the GISP2 isotope series.

Figure 8. ARfit spectral analysis of Absolute Intensity (green) record for the Holocene off D13892. 97.5% and 99.5% confidence intervals are shown.

Table Captions

Table1a and b. *Radiocarbon datings (1a) and tie-points (1b) used in development of D13892 chronology. The OXCAL calibration system was used for conversion of conventional radiocarbon dates to calendar years*

Figure Captions

Figure 1. Sediment facies of the Gulf of Cadiz contourite drift as revealed by sidescan sonar data. Location of D13892 is indicated. Modified from Hernandez-Molina et al., (2003).

Figure 2. Chronostratigraphy for D13892. Unbroken line indicates initial chronostratigraphic model, broken line indicates chronostratigraphy after tuning to GISP2 chronology (see Fig. 3)

Figure 3. Artificial Neural Network Sea Surface Temperature and $\delta^{18}O_{N.\ .pachyderma\ (d)}$ records for D13892 relative to GISP2 $\delta^{18}O$ record. Correlation points are shown.

Figure 4. Relationship of climate proxy and colour records in D13892 with GISP2 isotope series. Grey represents GISP2 $\delta^{18}O$, black represents $\delta^{18}O_{N.\ pachyderma\ (d)}$ for D13892. Coloured lines represent red-green-blue intensities, with upper curves indicating relative contribution to colour and lower curves indicating absolute intensity.

BLACK AND WHITE VERSION

Figure 4. Relationship of climate and colour in D13892 records. Grey area represents GISP2 $\delta^{18}O$. a) Relative intensity (red); b) Relative intensity (green); c) Relative intensity (blue); d) Absolute intensity (red); e) Absolute intensity (green); f) Absolute intensity (blue); g) $\delta^{18}O_{N.\ pachyderma\ (d)}$ for D13892.

Figure 5. Raw and transformed colour data for D13892. a) Absolute intensity in green wavelengths; b) Reflectance (L*); c) Relative Intensity (red); d) Chromaticness (C); e) Hue (H^o)

Figure 6. First differential of reflectance of representative samples from D13892, derived from Minolta spectrophotometer measurements. Interpretation of primary controls on reflectance intensities follows Giosan *et al.* 2002. Characteristic peaks in reflectance spectra, identified by statistical analysis of sediment core material analysed by colour and geochemical methods, are found for carbonate (400-500nm), haematite (500-600nm) and the reduced free iron (600-700nm).

Figure 7. Colour, geochemical and tests/gram data for D13892 relative to the GISP2 isotope series.

Figure 8. ARfit spectral analysis of Absolute Intensity (green) record for the Holocene off D13892. 97.5% and 99.5% confidence intervals are shown.

Table Captions

Table1a and b. *Radiocarbon datings (1a) and tie-points (1b) used in development of D13892 chronology. The OXCAL calibration system was used for conversion of conventional radiocarbon dates to calendar years*

Figure 1

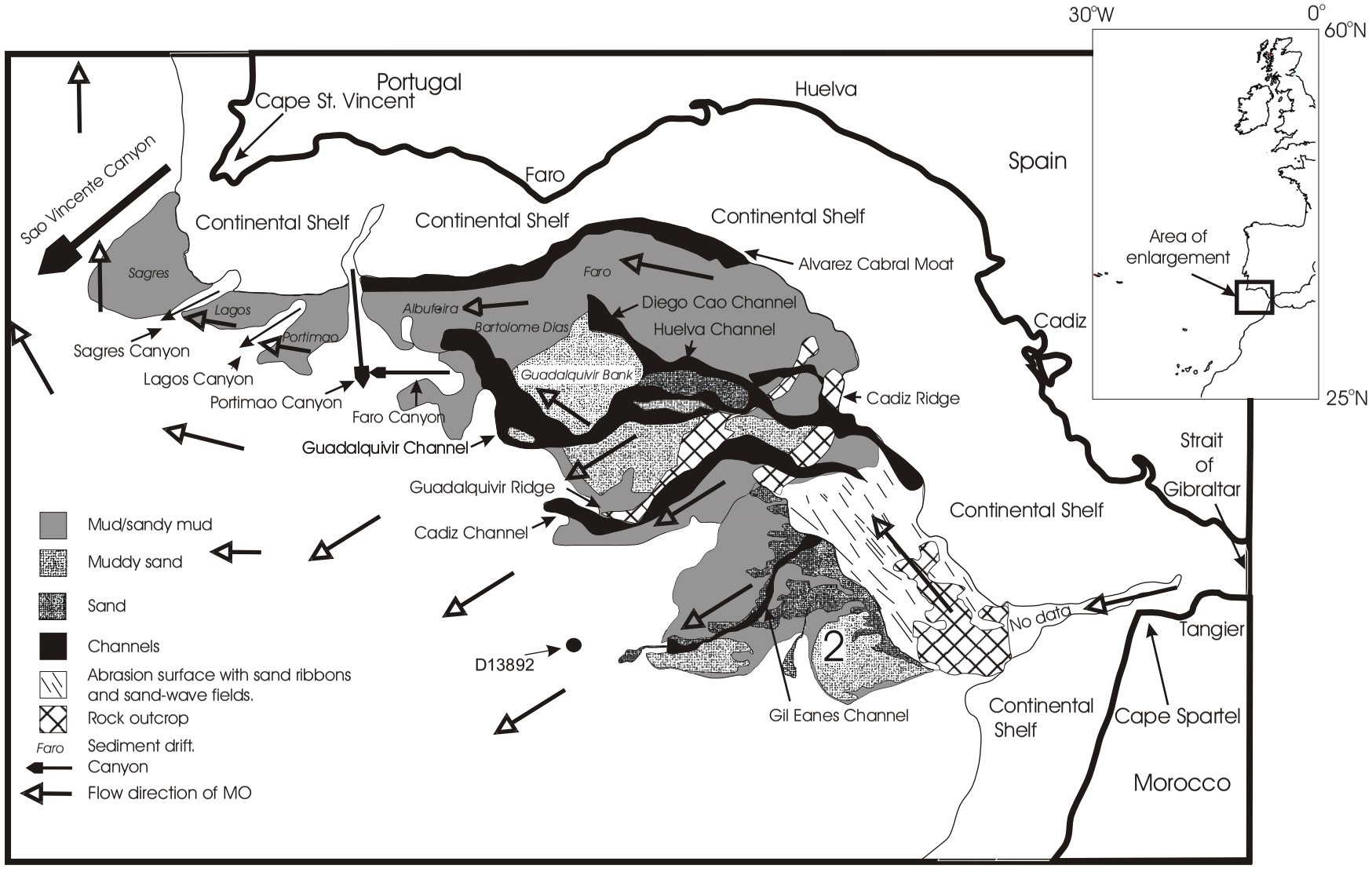
30°W
0°
60°N
25°N
Area of enlargement
Portugal
Cape St. Vincent
Huelva
Spain
Faro
São Vicente Canyon
Continental Shelf
Continental Shelf
Continental Shelf
Alvarez Cabral Moat
Sagres
Lagos
Portimao
Albufeira
Bartolome Dias
Faro
Diego Cao Channel
Huelva Channel
Cadiz
Sagres Canyon
Lagos Canyon
Portimao Canyon
Faro Canyon
Guadalquivir Bank
Cadiz Ridge
Guadalquivir Channel
Strait of Gibraltar
Guadalquivir Ridge
Cadiz Channel
Continental Shelf
Mud/sandy mud
Muddy sand
Sand
Channels
Abrasion surface with sand ribbons and sand-wave fields.
Rock outcrop
Faro
Sediment drift.
Canyon
Flow direction of MO
D13892
2
No data
Tangier
Gil Eanes Channel
Continental Shelf
Cape Spartel
Morocco

Figure 2.

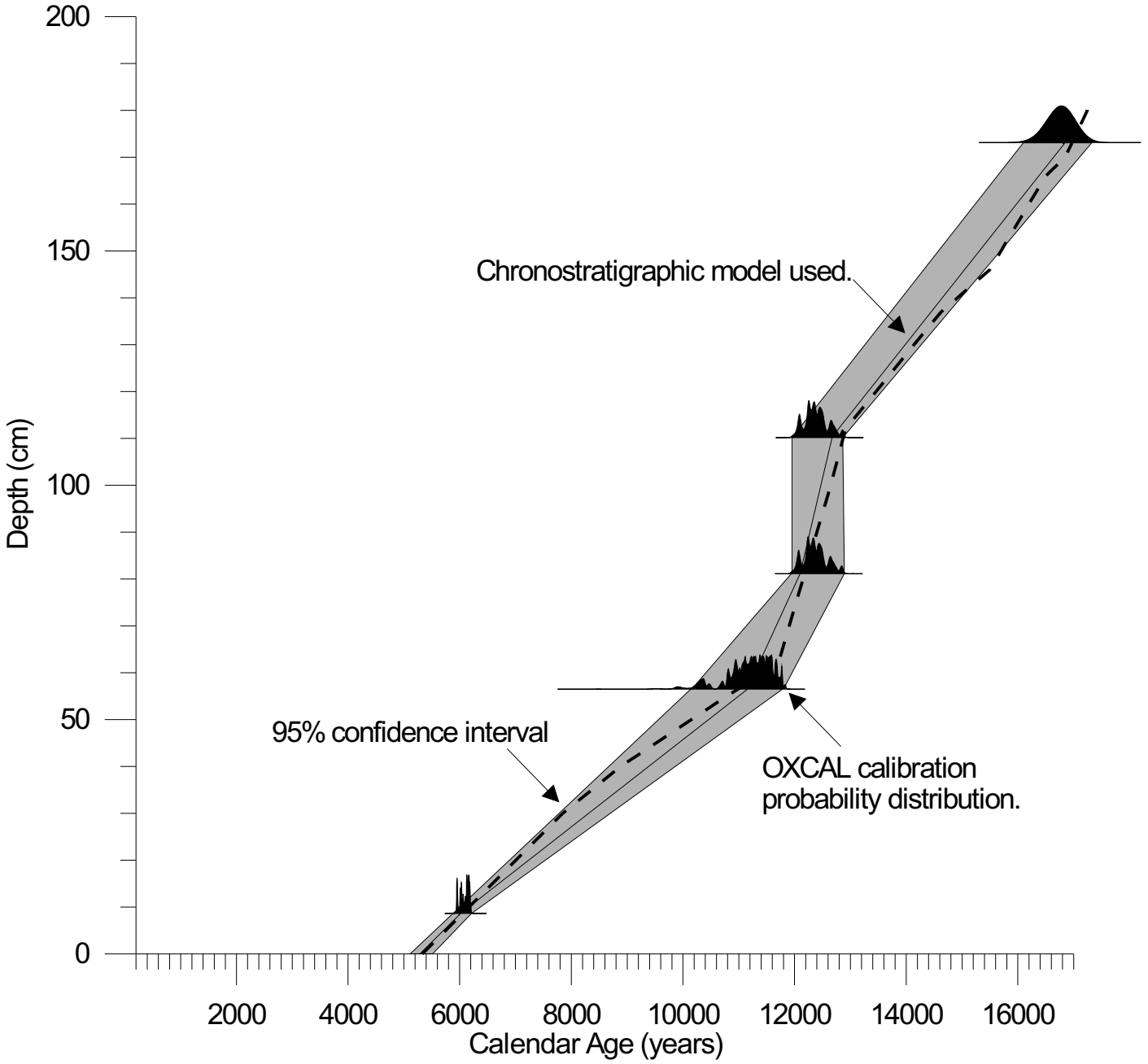
200
150
100
50
0
Depth (cm)
2000
4000
6000
8000
10000
12000
14000
16000
Calendar Age (years)
Chronostratigraphic model used.
95% confidence interval
OXCAL calibration
probability distribution.

Figure 3

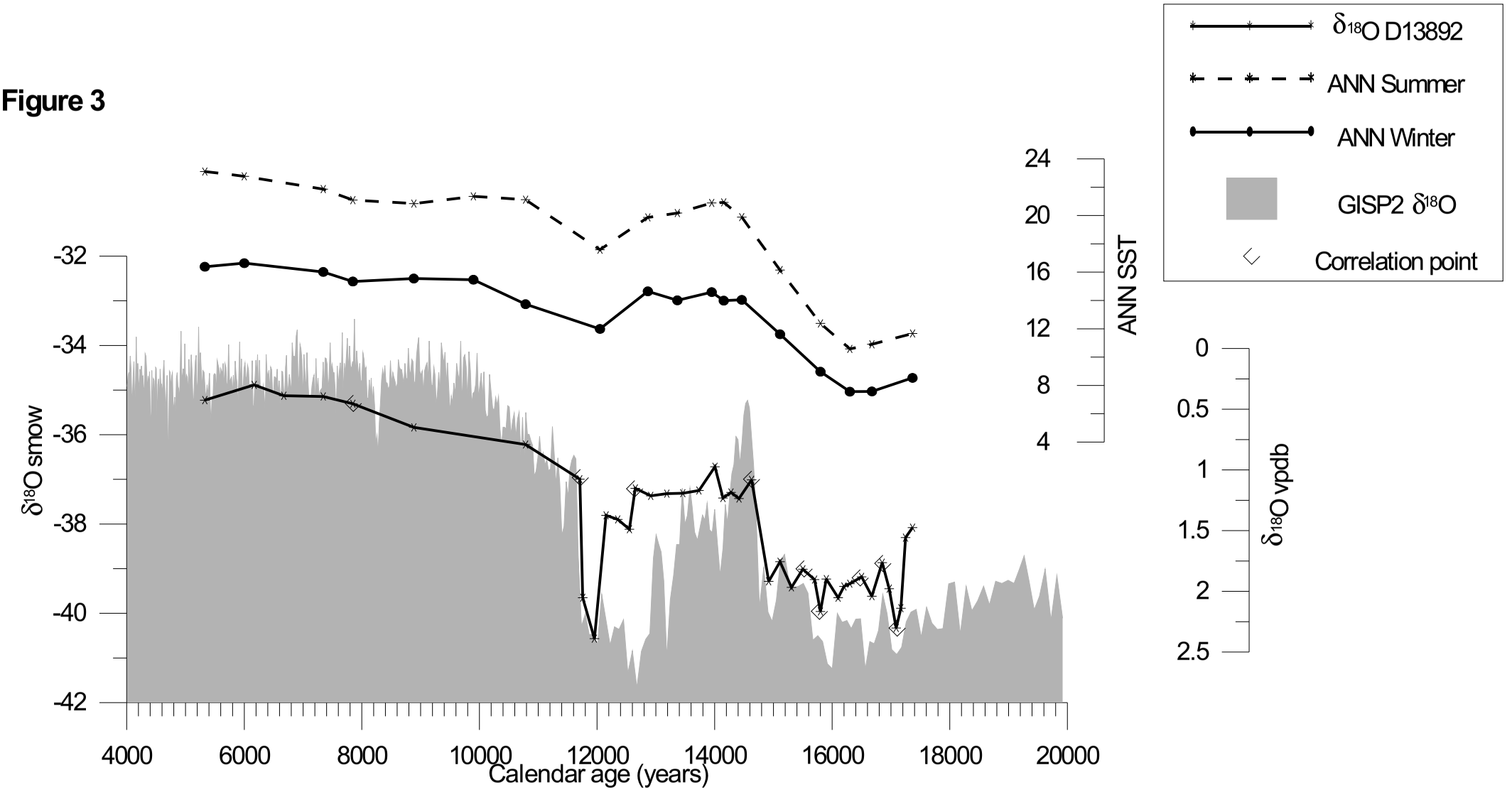
δ18O D13892
ANN Summer
ANN Winter
GISP2 δ18O
Correlation point
δ18O smow
-32
-34
-36
-38
-40
-42
ANN SST
24
20
16
12
8
4
δ18O vpdb
0
0.5
1
1.5
2
2.5
4000
6000
8000
10000
12000
14000
16000
18000
20000
Calendar age (years)

Figure 4

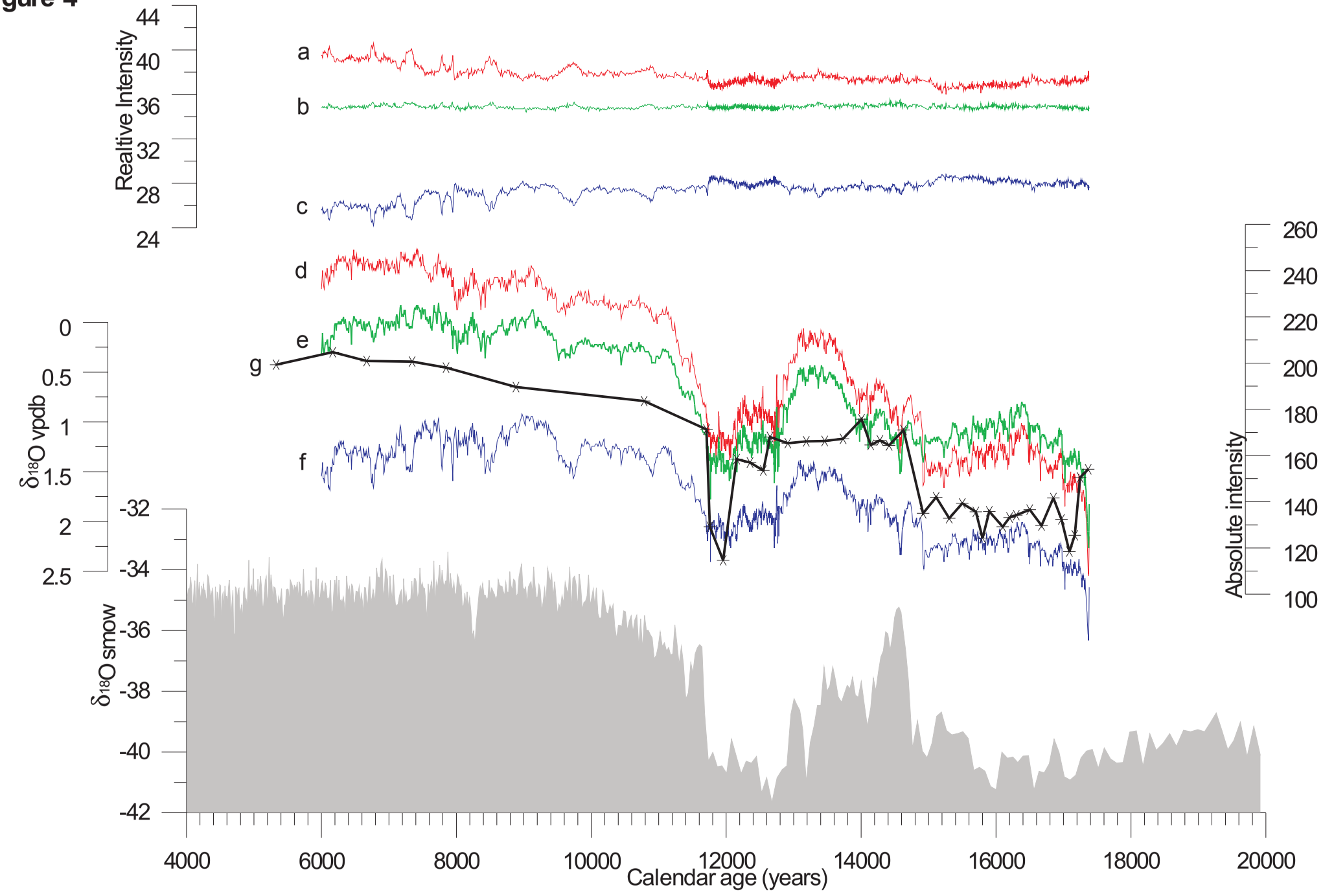
Realtive Intensity
44
40
36
32
28
24
a
b
c
d
e
g
f
δ18O vpdb
0
0.5
1
1.5
2
2.5
δ18O smow
-32
-34
-36
-38
-40
-42
Absolute intensity
260
240
220
200
180
160
140
120
100
4000
6000
8000
10000
12000
14000
16000
18000
20000
Calendar age (years)

Figure 5

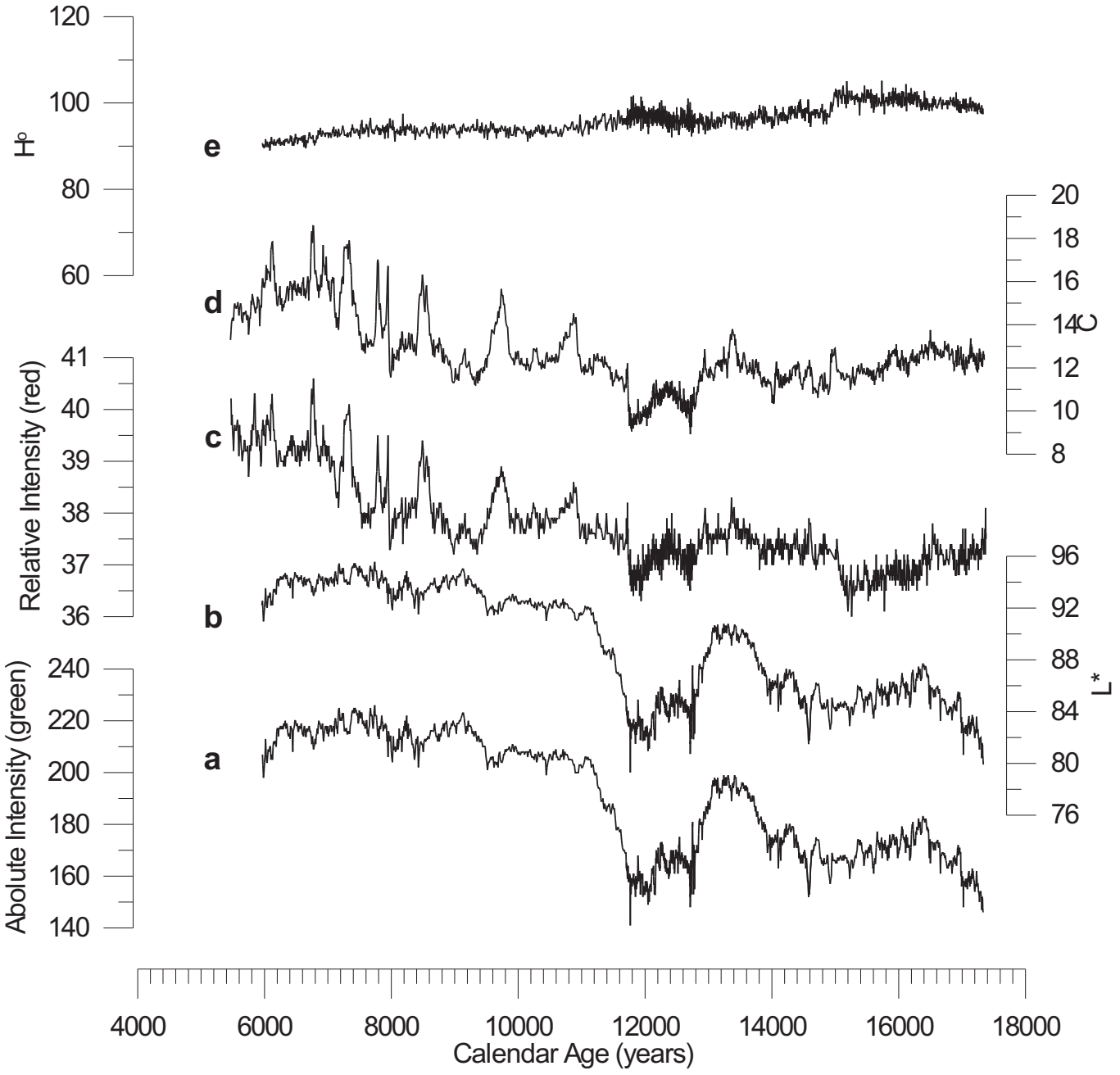
120
100
80
60
H°
e
d
c
b
a
41
40
39
38
37
36
Relative Intensity (red)
240
220
200
180
160
140
Abolute Intensity (green)
20
18
16
14
12
10
8
C
96
92
88
84
80
76
L*
4000
6000
8000
10000
12000
14000
16000
18000
Calendar Age (years)

Figure 6

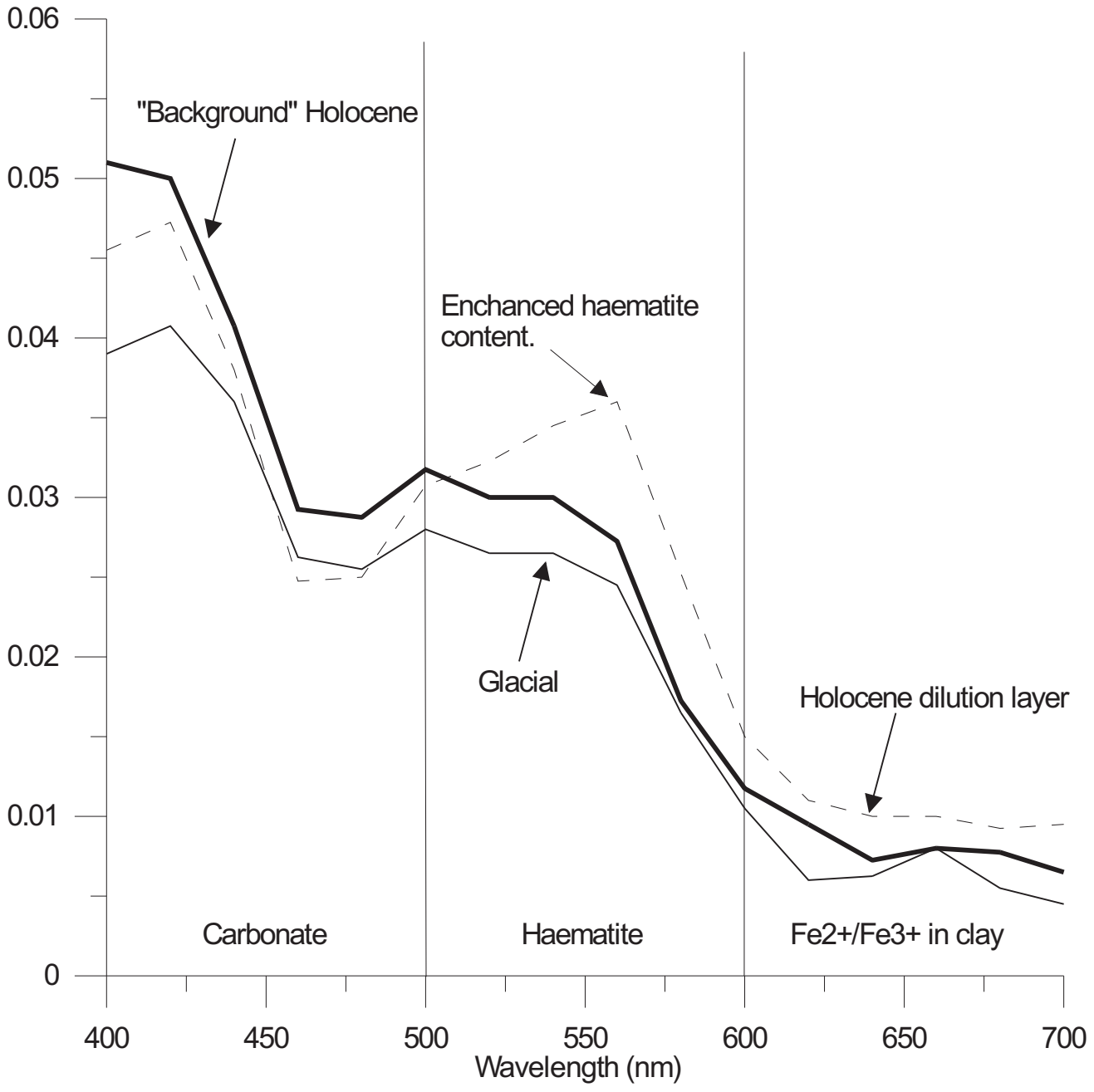
0.06
0.05
0.04
0.03
0.02
0.01
0
"Background" Holocene
Enchanced haematite content.
Glacial
Holocene dilution layer
Carbonate
Haematite
Fe2+/Fe3+ in clay
400
450
500
550
600
650
700
Wavelength (nm)

Figure 7

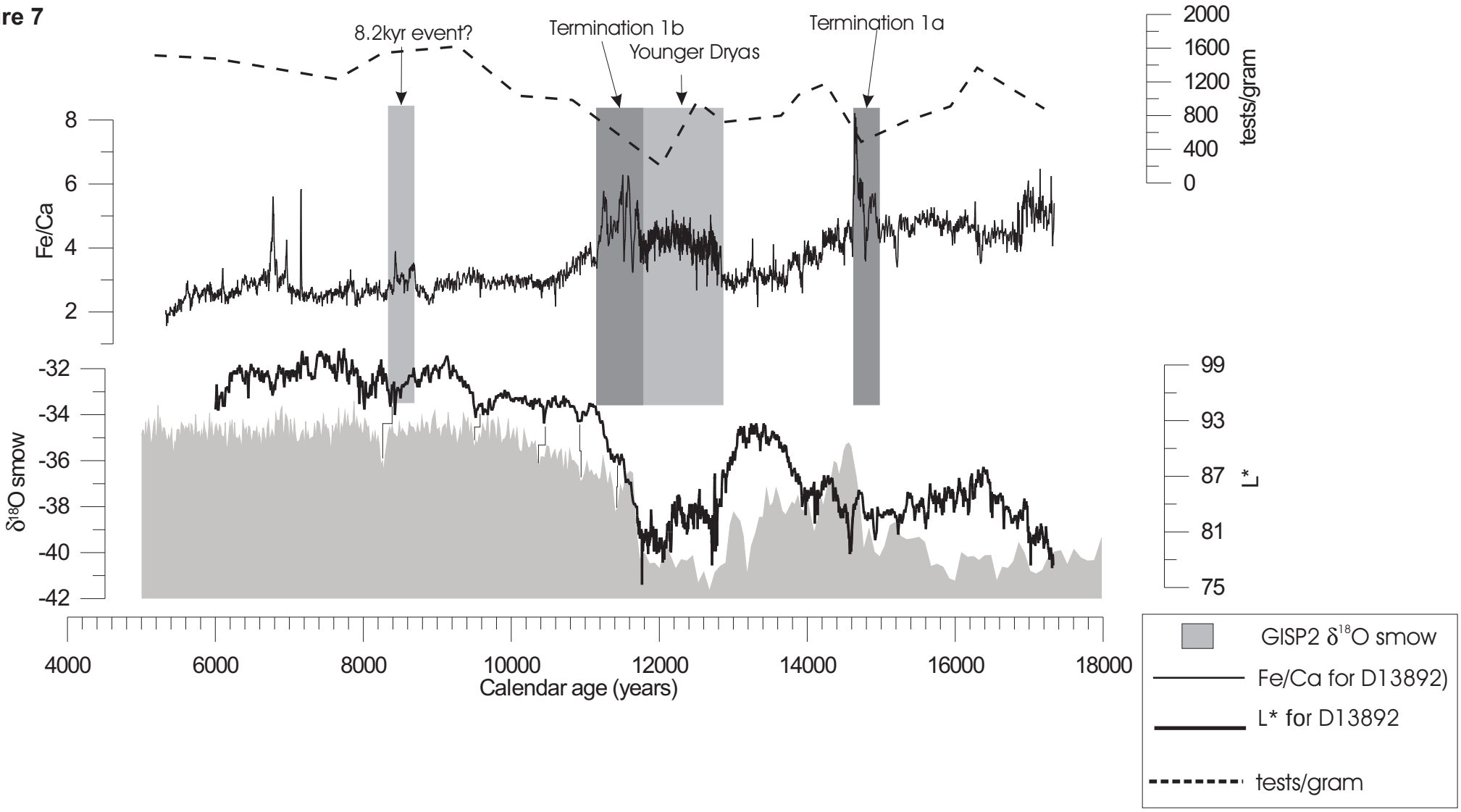
8.2kyr event?
Termination 1b
Younger Dryas
Termination 1a
Fe/Ca
tests/gram
δ18O smow
L*
Calendar age (years)
GISP2 δ18O smow
Fe/Ca for D13892)
L* for D13892
tests/gram

Figure 8

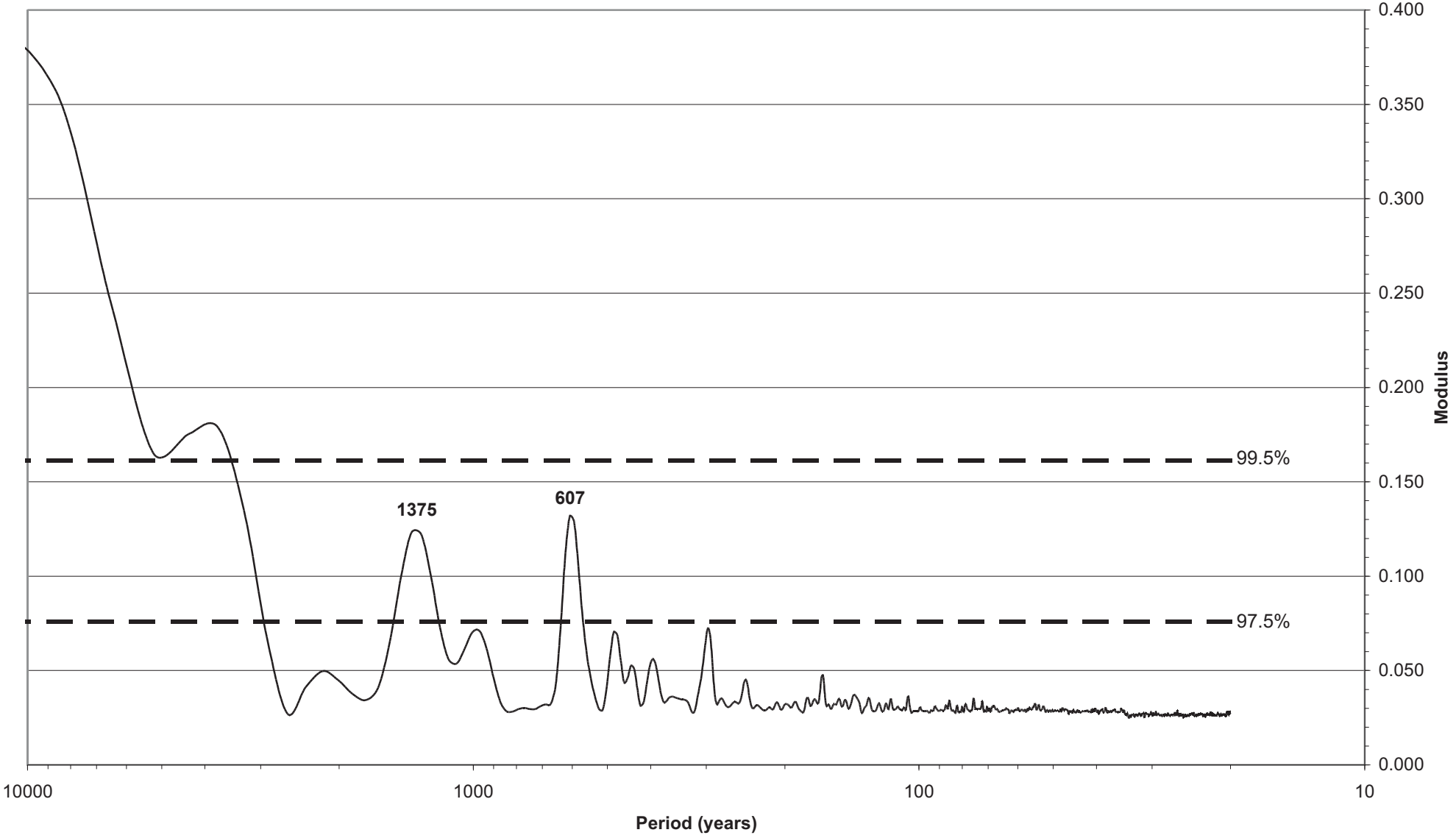
0.400
0.350
0.300
0.250
0.200
0.150
0.100
0.050
0.000
Modulus
99.5%
97.5%
1375
607
10000
1000
100
10
Period (years)